Effect of Production Time on Energy Use of a Tube-Ice Making Tower

Chittin Tangthieng
Department of Mechanical Engineering, Faculty of Engineering, Chulalongkorn University, Phayathai Road, Pathum Wan, Bangkok, 10330, Thailand
E-mail: fmectt@eng.chula.ac.th

Abstract

One of the important industries for a tropical country is the ice-making industry. In particular, tube ice is a form of ice for consuming, which is available in many grocery stores. This research is a numerical study of the effect of the production cycle time on the energy use of a tube-ice making process. The system is assumed one dimensional in the radial direction and unsteady. The governing equations are composed of the wall and the ice regions. The boundary condition at the wall surface is a convective type whereas the boundary condition at the interface is a isothermal solidification. The governing system is transformed into a dimensionless form, which is numerically solved by the finite difference method. The numerical solution in terms of ice thickness is compared with the data measured from the ice factory. There is a qualitative agreement between the numerical prediction and data obtained from the field measurement. From the numerical prediction, it can be seen that the average energy consumption is increased by approximately 5.8 kJ/m per minute with increase of the production cycle time. On the other hand, as the production cycle time increases, the average specific energy consumption reaches a minimum value of 0.341 kJ/g at a production cycle time of 14 minutes. Reduction of the production cycle time from 28 to 14 minutes leads to the higher value of the average specific energy consumption by 0.7 percent.

Keywords: tube ice, numerical method, production cycle time, energy consumption

1. Introduction

Tube ice is one of the important consuming products, especially for a tropical country. Because of its hygiene, tube ice is a favorable product for most consumers. Nevertheless, the limitation of the ice making industry is the transportation over a long distance. Therefore, tube-ice making industries are considered local ones, which are well-distributed in most of the districts in the country.

In a tube-ice making plant, the tube-ice making tower, which is serves as an evaporator of the refrigeration system, is a major component to product tube ice. Figure 1 illustrates the components of the tube-ice making tower. In general, the refrigerant is ammonia, and the saturation temperature is set at -8^{o}C. Heat transfer occurs between ammonia and liquid water through the tube. The liquid water is circulated by being pumped to the top of the tower, and it falls down to the bottom sump by gravity. Make-up water is added to compensate for the formation of ice. The tube is usually made of stainless steel with a nominal diameter of 1¼ inch.

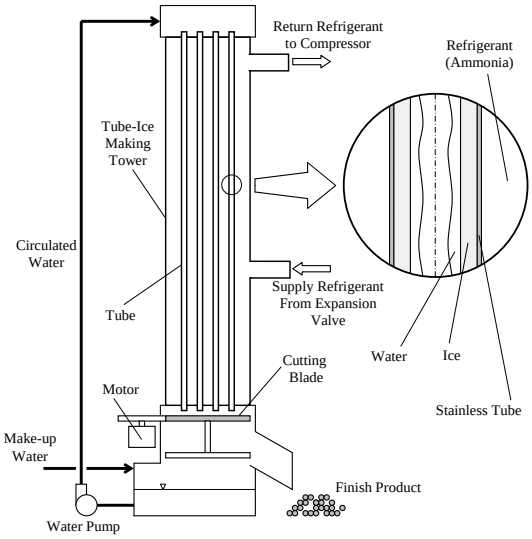

Figure 1 Components of tube-ice making tower

During tube-ice production, ice will form on the inner surface of the tube and grow until the diameter of the inner core is approximately 1 cm. Thereafter, the defrost process begins, and the tube ice is cut to a desired length by falling through a cutting blade at the bottom. The total production cycle is approximately 28 minutes, whereas the defrost period takes only 5 to 10 minutes.

In this study, a numerical method is employed to predict the average energy consumption, and the average specific energy consumption (SEC) of the tube-ice making process. a comparison between the numerical predictions and the field data is made. The effect of the different production cycle time on the average energy consumption and the average SEC is investigated. The results of this research may be used as a guideline to improve the energy efficiency of the tube-ice making process.

2. Problem Formulation

To formulate the mathematical model, the major assumptions for the tube-ice making process are made as follows: (i) The problem is one dimensional and transient. (ii) The interface where solidification takes place is sharp and isothermal at T_f. (iii) Ammonia is at the saturation temperature, T_0, with a convective heat transfer coefficient of h. (iv) The initial temperature of the tube is also at T_0. (v) Convection of liquid water is neglected. The schematic diagram of the tube-ice making problem is shown in Figure 2.

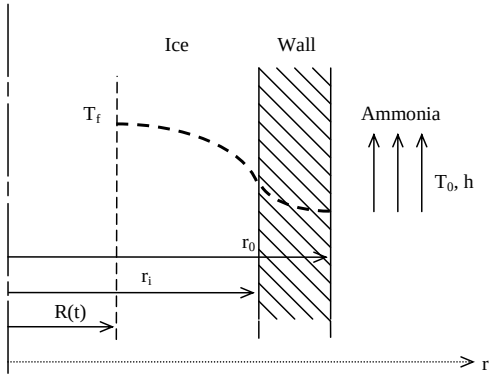

Figure 2 The schematic diagram of the problem under consideration

According to these assumptions, the mathematical models for the tube-ice making process are [1]:

(i) Ice Region

$$\frac{1}{\alpha_s}\frac{\partial T_s}{\partial t} = \frac{\partial^2 T_s}{\partial r^2} + \frac{1}{r}\frac{\partial T_s}{\partial r} \quad (1)$$

$$r = R(t);\ T_s = T_f,\ k_s\frac{\partial T_s}{\partial r} = \rho_s \Delta H \frac{dR}{dt} \quad (2a)$$

$$r = r_i;\ T_s = T_w,\ k_s\frac{\partial T_s}{\partial r} = k_w\frac{\partial T_w}{\partial r} \quad (2b)$$

$$t = 0;\ R(0) = r_i \quad (2c)$$

(ii) Wall Region

$$\frac{1}{\alpha_w}\frac{\partial T_w}{\partial t} = \frac{\partial^2 T_w}{\partial r^2} + \frac{1}{r}\frac{\partial^2 T_w}{\partial r^2} \quad (3)$$

$$r = r_i;\ T_s = T_w,\ k_s\frac{\partial T_s}{\partial r} = k_w\frac{\partial T_w}{\partial r} \quad (4a)$$

$$r = r_0 ; -k_w \frac{\partial T_w}{\partial r} = h\left(T_w - T_0\right) \quad (4b)$$

$$t = 0 ;\ T_w = T_0 \quad (4c)$$

3. Mathematical Analysis

To facilitate the computational procedure, a coordinate transformation is employed to the governing equations by introducing the following dimensionless variables:

$$\hat{t} = \frac{\alpha_s t}{(r_0 - r_i)^2} = \frac{\alpha_s t}{D^2} \quad (5)$$

$$\hat{r}_s = \frac{r - r_i}{r_i - R(t)} \quad (6)$$

$$\hat{r}_w = \frac{r - r_i}{r_0 - r_i} \quad (7)$$

$$\varphi = \frac{r_i - R(t)}{r_0 - r_i} = \frac{r_i - R(t)}{D} \quad (8)$$

$$\theta_s = \frac{T_s - T_0}{T_f - T_0} \quad (9)$$

$$\theta_w = \frac{T_w - T_0}{T_f - T_0} \quad (10)$$

Substituting the dimensionless variables into equations (1-4) gives:

(i) Ice Region

$$\frac{\partial^2 \theta_s}{\partial \hat{r}_s^{\,2}} + \frac{\varphi}{\hat{r}_s \varphi + R_r} \frac{\partial \theta_s}{\partial \hat{r}_s} + \left(\hat{r}_s \varphi \frac{d\varphi}{d\hat{t}}\right) \frac{\partial \theta_s}{\partial \hat{r}_s} - \varphi^2 \frac{\partial \theta_s}{\partial \hat{t}} = 0 \quad (11)$$

$$\hat{r}_s = 0;\ \theta_s = \theta_w, \frac{\partial \theta_s}{\partial \hat{r}_s} - R_1 \varphi \frac{\partial \theta_w}{\partial \hat{r}_w} = 0 \quad (12a)$$

$$\hat{r}_s = -1; \quad \theta_s = 1\ , \ \frac{\partial \theta_s}{\partial \hat{r}_s} + \frac{\varphi}{Ste} \frac{d\varphi}{d\hat{t}} = 0 \quad (12b)$$

$$\hat{t} = 0 ; \varphi = 0 \quad (12c)$$

(ii) Wall Region

$$\frac{\partial^2 \theta_w}{\partial \hat{r}_w^{\,2}} + \frac{1}{\hat{r}_w + R_r} \frac{\partial \theta_w}{\partial \hat{r}_w} - \frac{R_2}{R_1} \frac{\partial \theta_w}{\partial \hat{t}} = 0 \quad (13)$$

$$\hat{r}_w = 0 ; \theta_s = \theta_w, \frac{\partial \theta_s}{\partial \hat{r}_s} - R_1 \varphi \frac{\partial \theta_w}{\partial \hat{r}_w} = 0 \quad (14a)$$

$$\hat{r}_w = 1 ; \frac{\partial \theta_w}{\partial \hat{r}_w} + Bi\, \theta_w = 0 \quad (14b)$$

$$\hat{t} = 0 ; \theta_w = 0 \quad (14c)$$

It can be seen that the moving boundary conditions (2b) at r=R(t) are transformed to the fixed boundary conditions (12b) at $\hat{r}_s = -1$, which are favorable to the numerical procedure [2]. In addition, five dimensionless parameters appearing in equations (11-14) are:

$$R_1 = \frac{k_w}{k_s} \quad (15)$$

$$R_2 = \frac{\rho_w C_{pw}}{\rho_s C_{ps}} \quad (16)$$

$$Ste = \frac{C_{ps}\left(T_f - T_0\right)}{\Delta H} \quad (17)$$

$$Bi = \frac{h\, D}{k_w} \quad (18)$$

$$R_r = \frac{r_i}{r_0 - r_i} = \frac{r_i}{D} \quad (19)$$

In this study, R_1, R_2 R_r and Ste are treated as constants, whereas Bi is not due to the convective heat transfer coefficient of the nucleate boiling.

4. Finite Difference Analysis

Equations (11-14) can be solved by using the finite difference method. Because of the parabolic partial differential equations (11-14), the fully implicit scheme is employed to ensure numerical stability [3]. The partial differential terms appearing in equations (11) and (13) are replaced with the finite difference approximation as

follows:

$$\frac{\partial^2\theta}{\partial\hat{r}^2} = \frac{\theta_{i+1}^{n+1} - 2\theta_i^{n+1} + \theta_{i-1}^{n+1}}{(\Delta\hat{r})^2} \quad (20)$$

$$\frac{\partial\theta}{\partial\hat{r}} = \frac{\theta_{i+1}^{n+1} - \theta_{i-1}^{n+1}}{2\Delta\hat{r}} \quad (21)$$

$$\frac{\partial\theta}{\partial\hat{t}} = \frac{\theta_i^{n+1} - \theta_i^{n}}{\Delta\hat{t}} \quad (22)$$

By substituting equations (20-22) into the governing equations (11-14) and rearranging, the finite difference equations for nodes at the different locations, i.e., the interior nodes, the interfacial node at $\hat{r}_s = \hat{r}_w = 0$, and the boundary node at $\hat{r}_w = 1$, become:

(i) Interior Nodes

$$\left(1 - K\frac{\Delta\hat{r}}{2}\right)\theta_{i-1}^{n+1} - \left(2 + L\frac{\Delta\hat{r}^2}{\Delta\hat{t}}\right)\theta_i^{n+1} + \left(1 + K\frac{\Delta\hat{r}}{2}\right)\theta_{i+1}^{n+1} = -\left(L\frac{\Delta\hat{r}^2}{\Delta\hat{t}}\right)\theta_i^{n} \quad (23)$$

For the ice region:

$$K = \frac{\varphi}{\hat{r}_s\varphi + R_r} + \hat{r}_s\varphi\frac{d\varphi}{d\hat{t}},\ L = \varphi^2, \Delta\hat{r} = \Delta\hat{r}_s,\ \theta = \theta_s \quad (24)$$

For the wall region:

$$K = \frac{1}{\hat{r}_w + R_r},\ L = \frac{R_2}{R_1},\ \Delta\hat{r} = \Delta\hat{r}_w,\ \theta = \theta_w \quad (25)$$

(ii) Interfacial Node ($\hat{r}_s = \hat{r}_w = 0$) [4]

$$\left(1 - \frac{K_b\Delta\hat{r}_b}{2}\right)\theta_{i-1}^{n+1} - \left[\left(\frac{\Delta\hat{r}_a}{\Delta\hat{r}_b} + \frac{L_b\Delta\hat{r}_a\Delta\hat{r}_b}{2\Delta\hat{t}}\right)\left(1 + \frac{K_a\Delta\hat{r}_a}{2}\right)\frac{J_b}{J_a} + \left(1 + \frac{L_a\Delta\hat{r}_a^2}{2\Delta\hat{t}}\right)\left(1 - \frac{K_b\Delta\hat{r}_b}{2}\right)\right]\theta_i^{n+1} + \left(1 + \frac{K_a\Delta\hat{r}_a}{2}\right)\left(\frac{J_b\Delta\hat{r}_a}{J_a\Delta\hat{r}_b}\right)\theta_{i+1}^{n+1} = -\left[\left(\frac{L_a\Delta\hat{r}_a^2}{2\Delta\hat{t}}\right)\left(1 - \frac{K_b\Delta\hat{r}_b}{2}\right) + \left(\frac{L_b\Delta\hat{r}_a\Delta\hat{r}_b}{2\Delta\hat{t}}\right)\left(1 + \frac{K_a\Delta\hat{r}_a}{2}\right)\frac{J_b}{J_a}\right]\theta_i^{n} \quad (26)$$

where

$$K_a = \frac{\varphi}{R_r},\ L_a = \varphi^2,\ J_a = 1,\ \Delta\hat{r}_a = \Delta\hat{r}_s, \theta = \theta_s = \theta_w,$$

$$K_b = \frac{1}{R_r},\ L_b = \frac{R_2}{R_1},\ J_b = R_1\varphi,\ \Delta\hat{r}_b = \Delta\hat{r}_w \quad (27)$$

(iii) Boundary Node ($\hat{r}_w = 1$)

$$2\theta_{w,i-1}^{n+1} - \left(2 + L\frac{\Delta\hat{r}_w^{\,2}}{\Delta\hat{t}} + 2\,Bi\,\Delta\hat{r}_w\left(1 + K\frac{\Delta\hat{r}_w}{2}\right)\right)\theta_{w,i}^{n+1} = -\left(L\frac{\Delta\hat{r}_w^{\,2}}{\Delta\hat{t}}\right)\theta_{w,i}^{n} \quad (28)$$

where

$$K = \frac{1}{1 + R_r},\ L = \frac{R_2}{R_1} \quad (29)$$

Equations (23-29) are a set of nonlinear equations due to the appearance of φ and $d\varphi/dt$ terms. Thus, to linearize the equations, those two terms must be replaced by an approximation as follows:

$$\varphi = \frac{\varphi_i^{n+1} + \varphi_i^{n}}{2} \quad (30)$$

$$\frac{d\varphi}{d\hat{t}} = \frac{\varphi_i^{n+1} - \varphi_i^{n}}{\Delta\hat{t}} \quad (31)$$

By substituting equations (30-31) into equations (23-29), a set of these equations will be linearized in the form of a tridiagonal system. They can be solved by using Thomas algorithm. Note that an initial estimation of φ_i^{n+1} is required to run the numerical scheme. To verify the value of φ_i^{n+1}, the boundary condition (12b) will be utilized and be rewritten in a finite difference form.

$$\varphi_i^{n+1} = \sqrt{\varphi_i^{n\,2} + \left(\frac{Ste\,\Delta\hat{t}}{\Delta\hat{r}_s}\right)\left(\theta_{s,i+2}^{n+1} - 4\theta_{s,i+1}^{n+1} + 3\theta_{s,i}^{n+1}\right)} \quad (32)$$

The value of φ_i^{n+1} will be iterated until convergence.

It is noticed that Bi can be written as a function of h, which is no longer a constant due to nucleated boiling. In this case, the Stefan and Abdelsalan correlation [5] is utilized. By substituting the properties of ammonia [6] into this correlation, h for the nucleated boiling of ammonia at the saturation temperatures of -8^oC can be written as:

$$h = 6.307\times10^6 \left(\frac{T_{w,0} - T_0}{T_0}\right)^{2.0303} \quad (33)$$

The subscript w,0 represents the outer surface temperature of the tube. Rewriting equation (33) into a dimensionless form yields:

$$Bi = 1.304\,\theta_{w,0}^{2.0303} \quad (34)$$

During the computational scheme, Bi will be iterated until convergence. When both φ_i^{n+1} and Bi have converged, the program will record the temperature profile and the ice thickness, and then proceed to the next time step until the final (or production cycle) time, where ice thickness is approximately 12.5 mm, is reached.

It should be noted here that the physical initial condition at $\hat{t} = 0$ is a singularity due to the zero ice thickness, and it cannot be used as an initial condition for the numerical scheme. To avoid this difficulty, the numerical initial condition must be shifted to initial time at $\hat{t} << 1$, at which the radius of curvature of the tube is much greater than the ice thickness. The temperature distribution and the ice thickness at $\hat{t} << 1$ can be determined by the similarity solution [7].

The values of R_1, R_2, and Ste can be determined by substituting the properties of stainless steel and properties of ice given in Tables 1 and 2 into equations (15-17). For the value of R_r, the inner diameter of a standard 1¼-inch tube is 35.04 mm with the wall thickness of 3.56 mm. As a result, the values R_1, R_2, Ste, and R_r are:

$$R_1 = 7.158,\ R_2 = 1.863,$$
$$Ste = 0.0485,\ R_r = 4.921 \quad (35)$$

Table 1 Properties of ice [8]

Properties	**Values**
ρ_s (kg/m^3)	920
k_s (W/m-K)	1.91
C_{ps} (kJ/kg-K)	2.022
ΔH (kJ/kg)	333.7

Table 2 Properties of stainless steel [8]

Properties	**Values**
ρ_w (kg/m^3)	7,900
k_w (W/m-K)	14.1
C_{pw} (kJ/kg-K)	0.451

The computational results are represented in terms of the average energy consumption (EC_{avg}) and the average specific energy consumption (SEC_{avg}) at different production cycle times. Mathematically, EC_{avg} is the integral of the cooling-transfer-rate curve over a given production cycle time (t_p) whereas the SEC_{avg} is the average integral of the SEC curve over a given production cycle time:

$$EC_{avg} = \int_{t=o}^{t=t_p} (\text{Cooling Transfer Rate})\,dt \quad (36)$$

$$SEC_{avg} = \frac{1}{t_p}\int_{t=o}^{t=t_p} (\text{SEC})\,dt \quad (37)$$

The cooling transfer rate is given by:

$$\text{Cooling Transfer Rate} = 2\pi r_0 \, h\,(T_{w,0} - T_0)$$

$$= 2\pi k_w (T_f - T_0)(R_r + 1)\,\text{Bi}\,\theta_{w,0} \qquad (38)$$

The SEC is defined as the ratio of the cooling transfer rate to the production rate, which is given by:

$$\text{Production Rate} = \rho_s \frac{dA_{ice}}{dt} = -2\pi\rho_s R \frac{dR}{dt}$$

$$= 2\pi \frac{k_s}{C_{ps}} (R_r - \psi) \frac{d\psi}{d\hat{t}} \qquad (39)$$

$$\text{SEC} = \frac{\text{Cooling Transfer Rate}}{\text{Production Rate}}$$

$$= \frac{C_{ps}(T_f - T_0) R_1 (R_r + 1)\,\text{Bi}\,\theta_{w,0}}{(R_r - \psi)(d\psi / d\hat{t})} \qquad (40)$$

5. Results and Discussion

To verify the validity of numerical results, a comparison between the ice thickness obtained from the numerical prediction and that obtained from the field data measuring is made and illustrated in Figure 3.

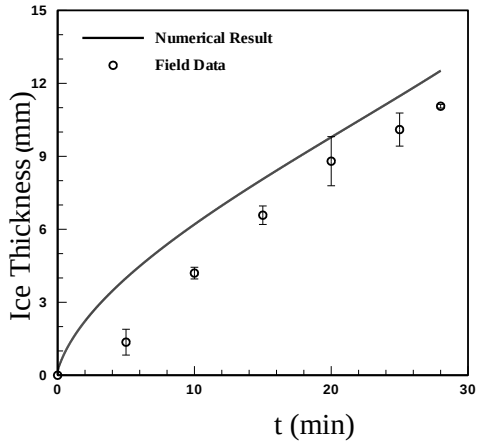

Figure 3 Comparison of the ice thickness obtained from two methods

In Figure 3, T_0 is set at -8^oC. It is noticed that both the numerical results and field data are in qualitative agreement. The ice thickness obtained from the numerical prediction is greater than that obtained from the field data. It is explained that the beginning of ice formation on the inner surface of the tube is not at t = 0 for the field data. This may stem from heat accumulation in the system after the defrost process. According to Figure 3, if the trend line is drawn based on the field data measurements, the trend line will intersect the horizontal axis at approximatedly 3 minutes. As a result, ice will be formed about 3 minutes after the beginning of the refrigeration process.

Figure 4 illustrates the relation of the cooling transfer rate obtained from the numerical prediction as a function of time. It can be seen that after the beginning of the process, the cooling transfer rate decreases rapidly. Thereafter, it will decrease at a slower rate at the end of the process. The reason is that the ice layer acts as if it is an insulator. As a result, the thicker the ice layer, the lower the cooling transfer rate from the ammonia to the liquid water.

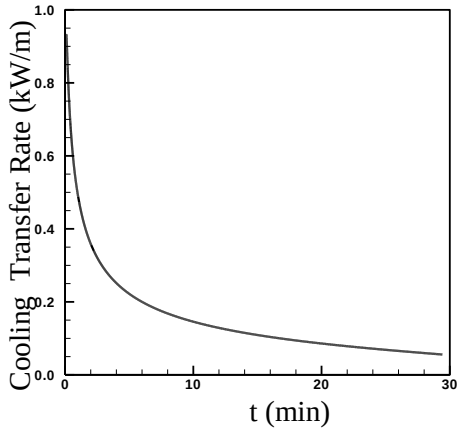

Figure 4 Variation of the cooling transfer rate with time

Figure 5 illustrates the relation of the SEC obtained from the numerical

prediction as a function of time. After the beginning of the process, the SEC first decreases, reaches a minimum point, and increases toward the end of process. It is explained that at the first part, the SEC decreases because the cooling transfer rate is still high leading to a high production rate. As time passes, the ice layer gets thicker and prevents the cooling effect from diffusing through the layer itself. Thus, the production rate gets lower, resulting in a higher value of SEC. The change of SEC over the entire production cycle is between 0.34 and 0.36 kJ/g. It should be noted that the lower the SEC, the more efficiently the energy is consumed. From Figure 5, if the ice-making process is terminated prior to the given production cycle time (i.e., 28 minutes), the value of SEC_{avg} should be lower. Thus, the relations between t_p and EC_{avg} and SEC_{avg} are investigated.

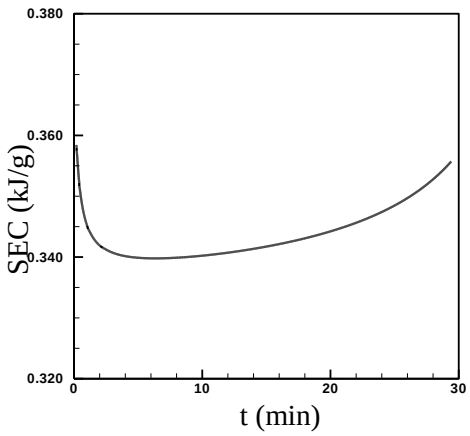

Figure 5 Variation of the specific energy consumption with time

The variation of EC_{avg} with different t_p is depicted in Figure 6. As expected, EC_{avg} increases with increasing t_p. By setting the value of EC_{avg} at t_p = 5 minutes as a reference case, EC_{avg} is increased by 48 and 108 percent when t_p increases from 5, to 10 and 20 minutes, respectively, with the average value of 5.8 kJ/m per minute.

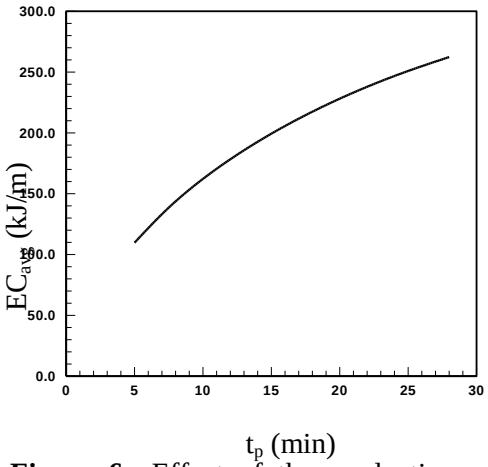

Figure 6 Effect of the production cycle time on the average energy consumption

The variation of SEC_{avg} with different t_p is depicted in Figure 7. SEC_{avg} decreases at the beginning when t_p is 5 minutes, reaches a minimum point, and increases until t_p reaches 28 minutes. Physically, SEC_{avg} represents the average energy consumption per mass of the produced ice over the entire cycle time. The lower the value of SEC_{avg}, the higher the energy efficiency of the process. According to Figure 7, the minimum point is located when t_p is approximately 14 minutes, with the minimum SEC_{avg} of 0.341 kJ/g. By comparing t_p at 14 minute with that at 28 minutes, the value of SEC_{avg} is decreased by 0.7 percent. In practice, the manufacturer tends to operate the ice-making system on the right side of the minimum point. Thus, it would be beneficial to the manufacturer to reduce the production cycle time from 28 minutes to 14 minutes, leading to a higher energy efficiency of the ice-making process. In the future, this numerical prediction can be adapted to different operating conditions, such as different tube diameters, refrigerant properties, or saturated refrigerant temperature to provide a proper production cycle time.

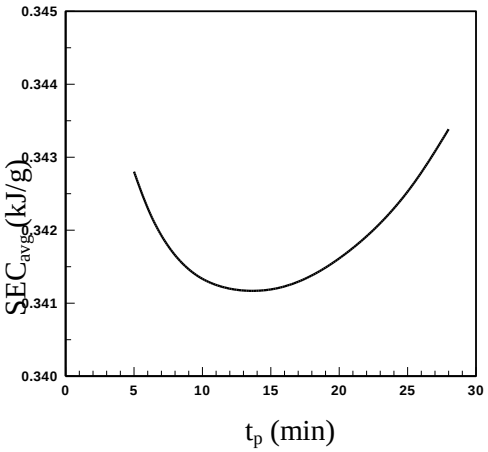

Figure 7 Variation of the average specific energy consumption with the production cycle time

6. Conclusions

In this study, a mathematical model of the tube-ice making process has been formulated. The finite difference approach is employed to solve the governing system. The numerical solutions to predict the average energy consumption and the average specific energy consumption as a function of the production cycle time are obtained. A comparison between the numerical predictions and the field data is made, which results in qualitative agreement. As the production cycle time increases, the average energy consumption is increased by approximately 5.8 kJ/m per minute, whereas the average specific energy consumption reaches a minimum value of 0.341 kJ/g at the production cycle time of 14 minutes. Based on this study, it is recommended for ice-making manufacturers to reduce the production cycle time from 28 to 14 minutes. This results in a higher value of the average specific energy consumption by approximately 0.7 percent.

7. Nomenclature

Bi Biot number
C_h constant in equation (33) [W/m^2-K]
C_p specific heat at constant pressure [J/kg-K]
C_{Bi} constant in equation (34)
D tube thickness [m]
EC energy consumption [kJ/m]
h convective heat transfer coefficient [W/m^2-K]
ΔH latent heat of fusion [J/kg]
k thermal conductivity [W/m-K]
J term for the finite difference equations
K term for the finite difference equations
L term for the finite difference equations
r distance in the radial direction [m]
r_i inner diameter of the tube [m]
r_0 outer diameter of the tube [m]
$\hat{r}$ dimensionless distance in the radial direction
R radius of the ice layer [m]
R_1 wall-to-ice heat capacity ratio
R_2 wall-to-ice thermal conductivity ratio
R_r ratio of the inner diameter to the tube thickness
SEC specific energy consumption [kJ/g]
Ste Stefan number
t time [s, min]
t_p production cycle time [min]
$\hat{t}$ dimensionless time
T temperature [^{o}C, K]

Greek Symbols

α thermal diffusivity [m^2/s]
φ dimensionless ice thickness
θ dimensionless temperature
ρ density [kg/m^3]

Subscripts

0 saturation state
avg average
f freezing point
s ice region
w wall region

8. References

[1] Necati Özisik, M., Heat Conduction, John-Wiley & Sons, New York, USA, pp. 416-430, 1993.

[2] Cheung, F. B. and Cha, S. W., Finite-Difference Analysis of Growth and Decay of a Freeze Coat on a Continuous Moving Cylinder, Numerical Heat Transfer, Vol. 12, pp. 41-56, 1987.

[3] Chapra, S. C. and Canale, R. P., Numerical Methods for Engineers, McGraw-Hill, New York, USA, pp. 738-741, 1990.

[4] Tangthieng, C, Cheung, F. B. and Shih, Y. C., Solidified Layer Growth and Decay Characteristics During Freeze Coating of a Binary Substance, Journal of Thermophysics and Heat Transfer, Vol. 16, pp. 379-388, 2002.

[5] Stephan, K. and Abdelsalam, M., Heat-Transfer Correlations for Natural Convection Boiling, International Journal of Heat and Mass Transfer, Vol. 23, pp. 73-87, 1980.

[6] Carey, V. P., Liquid-Vapor Phase-Change Phenomena: an Introduction to the Thermophysics of Vaporization and Condensation Processes in Heat Transfer Equipment, Taylor & Francis, USA, pp. 630, 1992.

[7] Piruchvet, N., and Tangthieng, C., A Numerical Study to Predict the Ice Thickness, the Ice Production Rate and the Cooling Load of the Block-Ice Making Process, the 18th Conference on Mechanical Engineering Network of Thailand, Article CST29, Khonkaen, Thailand, 18-20 October, 2005.

[8] Incropera, F. P. and Dewitt, D. P., Fundamentals of Heat and Mass Transfer, John-Wiley & Sons, New York, USA, pp. 905-916, 2002.